Beta-catenin

A molecular multiplayer

van der Wal, T.

Publication date
2024

6.

“So, so you think you can tell?”
– Pink Floyd

How to lose a guide in three years: a CRISPR optimizing story

Tanne van der Wal[1], Melanie Rietveld[1], Saskia M.A. de Man[1] & Renée van Amerongen[1]

[1] Developmental, Stem Cell and Cancer Biology, Swammerdam Institute for Life Sciences, University of Amsterdam, Science Park 904, 1098 XH Amsterdam, the Netherlands

Author's note

During the first three years of my PhD, I put much effort into creating functional point mutations in fluorescently tagged CTNNB1 with the ultimate goal of measuring the effects on its subcellular distribution via quantitative microscopy. Unfortunately, this project has remained unfinished due to practical difficulties encountered in the CRISPR editing phase. In this chapter, we describe our rationale and experimental design for introducing point mutations that should disturb the interaction of CTNNB1 with several of its binding partners, including CDH1 and CTNNA1. We also report our attempts to optimize a co-CRISPR approach for simultaneous tagging and mutating of CTNNB1 and the subsequent screening for successful edits. Finally, we narrate the bottlenecks we encountered while optimizing the (co)-CRISPR protocol in human breast epithelial (MCF10A) cells, such that others can build on this work in the future.

Introduction

In previous chapters, we artificially adjusted the balance of CTNNB1 by modulating either WNT signalling (chapter 4) or cell adhesion (chapter 5). In doing so, it has appeared challenging to experimentally uncouple the functions of CTNNB1. As highlighted in Chapter 1, CTNNB1 contains binding sites for many proteins - including the cell adhesion components cadherin (hereafter CDH) and CTNNA1, and the WNT pathway components TCF and AXIN/APC. As most of these binding sites overlap (see figure 3 in chapter 1), binding of cell adhesion versus WNT signalling components to CTNNB1 is typically thought to be mutually exclusive. We reasoned, therefore, that the most direct way to shift the balance of CTNNB1 between its two functions would be to reduce binding affinity for one or more of its interacting partners through the introduction of defined point mutations in CTNNB1.

We hypothesized that this approach might also allow us to separate the contribution of individual binding partners to its subcellular distribution and function. For example, disrupting the binding of CTNNA1 to CTNNB1, would probably still allow CTNNB1 to bind to CDH, whereas disturbances in cell adhesion would likely affect the CDH/CTNNA1/CTNNB1 complex as a whole. Using quantitative microscopy, it should be possible to detect subtle changes in functional localization of CTNNB1 in response to such point mutations. Here, it is important to create point mutations in the endogenous CTNNB1 locus, as overexpressing CTNNB1 could easily saturate the system. This would likely create a situation with excess levels of CTNNB1 compared to those of its binding partners, overruling any differences in binding affinity. As part of the regulatory mechanism behind balancing CTNNB1 between its two pools could be differences in binding affinity for the interacting partners, overexpression is not suitable for researching CTNNB1 balance.

CRISPR lends itself well for making endogenous point mutations, as shown in chapter 4, where an S45F mutation was created in the endogenous CTNNB1 locus (de Man et al., 2021). In this chapter, we initially set out to fluorescently tag and mutate endogenous CTNNB1 in human near-diploid breast epithelial cells (MCF10A). Since this posed unexpected bottlenecks, we resorted to testing some of our approaches in HAP1 cells. Altogether, the work described here summarizes our best efforts to optimize three critical steps in our experimental workflow: (i) experimental design and testing of gRNAs to mutate CTNNB1 residues Y142 and Y654, which are critical for CTNNA1 and CDH binding respectively, (ii) co-CRISPR for simultaneous fluorescent tagging and genetic editing of endogenous CTNNB1, and (iii) obtaining single-cell MCF10A clones following genetic editing and FACS sorting.

Materials and methods

Cell culture

The HEK293A cell line was used for plasmid transfection to test the guideRNA (gRNA) efficiency using Tracking of Indels by Decomposition (TIDE) analysis. HEK293A cells were cultured under 5% CO2 at 37˚C in Dulbecco's Modified Eagle Medium (DMEM) with glutamax (61965-026, Gibco) supplemented with 10% Fetal Bovine Serum (FBS) (10270106, Gibco). The HAP1 cell line was used to optimize conditions for efficient co-CRISPRing of a fluorescent marker and a point mutation. HAP1 WT (a kind gift from Thijn Brummelkamp (NKI), acknowledging the Whitehead institute as the source of the material), HAP1 SGFP2-CTNNB1 (de Man et al., 2021) and HAP1 SGFP2-CTNNB1^{S45F} cells (de Man et al., 2021) were maintained as described in chapter 4. MCF10A cells were used to optimize single cell FACS sorting and colony outgrowth for future CRISPR experiments in this cell line and were maintained as described in chapter 5. All cell lines were passaged every 2-3 days using 0.05% trypsin-EDTA (phenol red) (25300054, Gibco), 0.25% trypsin-EDTA (phenol red) (25200072, Gibco) and a 1:1 mix of 0.05% and 0.25% trypsin-EDTA for the HEK293A, HAP1, and MCF10A cell lines, respectively.

CRISPOR gRNA design for point mutations at Y142 and Y654

To create point mutations at residues Y142 and Y654 in human CTNNB1, CRISPOR software (Concordet & Haeussler, 2018) was used for the gRNA design. 200 bp regions surrounding the target codon (±100 bp on either side) were used as input for the CRISPOR *in silico* prediction tool (table 1), searching for 20bp gRNAs adjacent to an NGG PAM site and using the hg19 genome as a reference.

Table 1. CRISPOR input sequences

200 bp input sequences for CRISPOR in silico gRNA design for point mutations at residues Y142 and Y654. Target codons have been underlined in the sequence.

Target codon	Input sequence
Y142	5' - CCCATCTACACAGTTTGATGCTGCTCATCCCACTAATGTCCAGCGTTTGGCTGAACCATCACAGATGCTG AAACATGCAGTTGTAAACTTGATTAAC<u>TAT</u>CAAGATGATGCAGAACTTGCCACACGTGCAATCCCTGAAC TGACAAAACTGCTAAATGACGAGGACCAGGTAAGCAATGACATAGCTAGCTTTTTAGTCT – 3
Y654	5' - GTGGGTAAGTAAAAAGGAACCAAAGCCTTTAGCAGATGTGTACATTGAAGTCTCAGTTTTTCCTCAAG GGCCTTTTTCTCCTTGTCTCTTAGCGACA<u>TAT</u>GCAGCTGCTGTTTTGTTCCGAATGTCTGAGGACAAGCCA CAAGATTACAAGAAACGGCTTTCAGTTGAGCTGACCAGCTCTCTCTTCAGAACAGAGCCAA – 3'

gRNA cloning and efficiency testing using TIDE

Designed gRNAs (table 2) were optimized for cloning and expression into the pSpCas9(BB)-2A-Puro V2.0 (pX459) vector (a kind gift from the Feng Zang lab, available from Addgene, plasmid 362988) (Ran et al., 2013). If not present, a G was added to the 5' end of the gRNA to improve transcription by the U6 promoter. Additionally, CACC (forward) and AAAC (reverse) overhangs were added to aid ligation into a BbsI cut vector. The oligos were annealed and phosphorylated and the pX459 vector was cut with BbsI and dephosphorylated, after which the resulting products were ligated and transformed. Clones were tested via restriction enzyme digestion with HpaII and Sanger sequencing (primer 1278, table 2).

For TIDE analysis, 150,000 HEK293A cells were plated and transfected after 24 hours with 1500 ng gRNA construct or empty pX459 as a control in Optimem (31985070, Gibco), using 4.5 µg polyethylenimine (PEI) (23966-2, Polysciences) dissolved in Milli-Q. At 72 hours post transfection, genomic DNA was isolated from the cells. PCR amplification with DreamTaq (EP0701, Thermo Fisher) was used to amplify the region of interest surrounding the expected cut site (see table 2 for primers). PCR products were sequenced with the primers listed below table 2. Primers were designed according to the TIDE guidelines, targeting the region 200 bp before and 500 bp after the expected cut site (Brinkman et al., 2014).

Table 2. Oligos and primers for gRNA creation and testing

A summary of all the gRNA oligos and primers that were used for creating the pX459 vectors (listed with their plasmid codes) and for PCR amplification plus TIDE analysis, respectively.

RvA code	Target codon	Sequence	Usage	Plasmid code
2386	Y142	CACC GCAGTTCAGGGATTGCACGTG	gRNA oligo	pRvA238
2387	Y142	AAAC CACGTGCAATCCCTGAACTGC	gRNA oligo	pRvA238
2388	Y142	CACC GACAAAACTGCTAAATGACG	gRNA oligo	pRvA239
2389	Y142	AAAC CGTCATTTAGCAGTTTTGTC	gRNA oligo	pRvA239
3389	Y142	AGGTAAATGCTGAACTGTGGA	Primer (fwd)	N.A.
3390	Y142	GCTAAACGCACTGCCATTTT	Primer (rev)	N.A.
3391	Y142	AAATGCTGAACTGTGGATAGTGA	Primer (fwd)	N.A.
3392	Y142	AAACGCACTGCCATTTTAGC	Primer (rev)	N.A.
3396	Y654	CACC GAGCCGTTTCTTGTAATCTTG	gRNA oligo	pRvA297
3397	Y654	AAAC CAAGATTACAAGAAACGGCT	gRNA oligo	pRvA297
2390	Y654	CACC GTGGCTTGTCCTCAGACATT	gRNA oligo	pRvA240
2391	Y654	AAAC AATGTCTGAGGACAAGCCAC	gRNA oligo	pRvA240
2392	Y654	CACC GCATATGTCGCTAAGAGACA	gRNA oligo	pRvA241
2393	Y654	AAAC TGTCTCTTAGCGACATATGC	gRNA oligo	pRvA241
3393	Y654	GGCTTGCCATGTTTTAGCTT	Primer (fwd)	N.A.
3394	Y654	TGTTTCAAGGAACCACCTGT	Primer (rev)	N.A.
3395	Y654	CACCTGTACTGAGGACAAATGC	Primer (rev)	N.A.
1278	Other	GAGGGCCTATTTCCCATGATT	Px459 sequencing primer	N.A.

Repair template design

For the Y142E and Y654E mutations, repair templates were designed (Table 3). Regions of 100bp (±50 bp either side of the point mutation) were taken and edited to create the desired Y to E mutation at the target codons. For Y142E, a silent mutation to include a PacI restriction site (to allow rapid screening for successful edits via PCR and restriction enzyme digest) and a silent mutation at the PAM site (to prevent re-cutting after successful repair) were added. For Y654E, a silent mutation to include a XhoI restriction site was added. As for Y654E the gRNA overlaps with the target codon, no additional mutation needed to be made to remove the PAM site.

Table 3. Repair template design

The designed Y142E and Y654E repair templates. PacI (Y142E) and XhoI (Y654E) restriction sites are underlined and the point mutations Y142E and Y654E (TAT to GAA) are visible in bold. For Y142E, the PAM site mutation (CCA to CAA) is visible in small font.

Y142E	5’-TGGCTGAACCATCACAGATGCTGAAACATGCAGTTGTAAACTTAATTAACC**GAA**CAAGATGATG CAGAACTTGcaaCACGTGCAATCCCTGAACTGACAAA-3’
Y654E	5’-AGTCTCAGTTTTTCCTCGAGGGCCTTTTTCTCCTTGTCTCTTAGCGACA**GAA**GCAGCTGCTGTTTTGT TCCGAATGTCTGAGGACAAGCCACAAGATTAC-3’

Co-CRISPR trials and FACS analysis

800,000 wildtype HAP1 cells were seeded per 6-well, 24 hours prior to transfection with the CRISPR gRNA and repair constructs for creating a simultaneous SGFP2 knock-in and S45F point mutation (using the same constructs as previously described in de Man et al. 2021). Cells were transfected with different amounts and ratios of the CRISPR constructs in Optimem (31985070, Gibco) (see table 4), maintaining a maximum total DNA input of 2000 ng per well, using Turbofect (R0531, Thermo Fisher) according to the manufacturer’s instructions. For comparison, HAP1 SGFP2-CTNNB1 cells were transfected to introduce the S45F point mutation to reflect consecutive tagging and targeting. At 24 hours post transfection, cells were selected with 0.75 μg/ml puromycin (A1113803, Gibco) for a duration of 24 hours. The selected cells were then expanded and used for FACS analysis at day 11 post transfection.

For FACS analysis, cells were stained with 1 μg/ml DAPI (D1306, Invitrogen) in 2% HF (HBSS (14175053, Gibco) with 2% FBS (10270106, Gibco)) and subsequently washed and resuspended in 2% HF. Cells were kept on ice and filtered with a 70 μm cell strainer (10788201, Fisher Scientific) prior to analysis on a FACSARIA3 (BD Biosciences). Between 30,000 and 100,000 events were recorded per sample. Data was analyzed with FlowJo (version 10). The gating strategy is detailed in supplementary figure 1. For the co-CRISPR analysis, GFP^{negative}, GFP^{low}, and GFP^{high} gates were set based on HAP1 WT signal, HAP1 SGFP2-CTNNB1 and HAP1 SGFP2-CTNNB1^{S45F} signal, respectively. GFP^{low} and GFP^{high} gates were taken together for calculations using the total number of GFP^{positive} cells.

Table 4. Transfection scheme for co-CRISPR trials with SGFP2 and S45F

A summary of all the transfected combinations of the SGFP2 and S45F CRISPR. Both the ratio of pX-gRNA and the SGFP2 repair construct or S45F repair oligo as well as the SGFP2:S45F ratio was varied.

Cell line	SGFP2 CRISPR			S45F CRISPR			SGFP2:S45F ratio
	pX459-CTNNB1	pRepair -SGFP2	pX:repair ratio	pX459-S45F-CTNNB1	S45F oligo (10 mM)	pX:repair ratio	
HAP1 WT	500 ng	500 ng	1:1	500 ng	1 µl	1:1	1:1
HAP1 WT	500 ng	500 ng	1:1	500 ng	2 µl	1:1	1:1
HAP1 WT	333 ng	666 ng	1:2	333 ng	1.3 µl	1:2	1:1
HAP1 WT	666 ng	333 ng	2:1	666 ng	0.7 µl	2:1	1:1
HAP1 WT	333 ng	333 ng	1:1	666 ng	1.3 µl	1:1	1:2
HAP1 WT	666 ng	666 ng	1:1	333 ng	0.7 µl	1:1	2:1
HAP1 WT	250 ng	250 ng	1:1	750 ng	3 µl	1:1	1:3
HAP1 SGFP2-CTNNB1	-	-	-	1000 ng	2 µl	1:1	-
HAP1 SGFP2-CTNNB1	-	-	-	1000 ng	4 µl	1:2	-

CRISPR in MCF10A cells: single cell sorting and clonal expansion trials

For optimization of the CRISPR workflow in MCF10A cells, we aimed to create an mEos4B knock-in at the N-terminus of CTNNB1. The design of this knock-in was based on that of the sGFP2 knock-in as described by de Man et al. (2021), using the same pX459-CTNNB1-ATG gRNA. To create the mEos4B repair construct, we cloned mEos4B-N1 (54814, addgene) into the existing backbone with the CTNNB1 homology arms (pRvA111) as used by de Man et al. (2021) using Gibson assembly (primers for creating overhangs are shown in table 5).

For transfection, 150,000 MCF10A cells were seeded in 6-well plates. Cells were transfected with 2000 ng of different ratios (1:1, 1:2, 2:1) of mEos4b CRISPR gRNA and repair constructs in Optimem (31985070, Gibco) after 24 hours, using X-tremeGENE HP (6366546001, Roche) according to the manufacturer's instructions. As controls, pSGFP2-C1 and empty pX459 vectors were transfected. After 48 hours, cells were selected with 0.75 µg/ml puromycin (A1113803, Gibco) for a duration of 24 hours. Cells were then expanded for

7-10 days and prepared for FACS sorting.

Prior to FACS sorting, 50,000 WT MC10A cells were seeded into 96-wells plates and grown for 24 hours. MCF10A cells were prepared for FACS sorting as described in the section above. Gates were set based on MCF10A WT signal, which was set as $GFP^{negative}$. $GFP^{positive}$ cells were single cell sorted at 4˚C on a FACSARIA3 (BD Biosciences) into the 96-wells plate containing WT MCF10A cells. After sorting, plates were spun down at 1000 rpm for 4 minutes and expanded at 37˚C. After expansion, $GFP^{positive}$ cells were resorted from the population to remove the WT MCF10A cells and further expanded. Clones were then sequenced to confirm successful CRISPR events.

Single cell viability after sorting into 96-wells plates was an unexpected bottleneck that we attempted to optimize. In addition to sorting into a WT MCF10A population, we changed FACS buffer composition (HF percentage was increased to 4%), used conditioned medium to sort into, added 3-10 µM ROCK inhibitor Y-27632 (1254, Tocris) and gelatin (G9391, Sigma-Aldrich) or fibronectin (30 µg/ml, Sanquin) coated the sorting plates, as detailed in table 8.

Table 5. mEos4B CRISPR repair Gibson assembly overhang primers

Primers used for creating the CRISPR repair construct for N-terminal knock-in of mEos4B into CTNNB1, based on the design of the constructs to create the SGFP2-CTNNB1 knock-in. PCR was performed to create overhangs for Gibson assembly (overhangs are underlined).

RvA code	Target	Sequence	Usage
3377	mEos4B-N1	AATCCAGCGTGGACAATGGTGAGTGCGATTAAGC	Primer (fwd)
3378	mEos4B-N1	ACCTTGAGTAGCCATTCGTCTGGCATTGTCAGG	Primer (rev)
3379	Homology arm backbone (pRvA111)	GACAATGCCAGACGAATGGCTACTCAAGGTTTGTG	Primer (fwd)
3380	Homology arm backbone (pRvA111)	AATCGCACTCACCATTGTCCACGCTGGATTTTC	Primer (rev)

Results & Discussion

Rationale for mutation residues Y142 and Y654 in CTNNB1

We identified 2 candidate residues on CTNNB1 as eligible for mutation: Y142 and Y654. Each of these is postulated to lower the affinity of CTNNB1 for cell adhesion components.

Y142

Tyrosine residue Y142 has been found as a regulatory node for binding to both CTNNA1 and BCL9L (Aberle et al., 1994, 1996; Brembeck et al., 2004), which perform functions in cell adhesion and transcription respectively. Its phosphorylation (or phospho-mimic Y142E substitution) decreases CTNNA1 binding thereby promoting BCL9L binding. Y142 phosphorylation is not required for BCL9L binding (Hoffmans & Basler, 2007; Sampietro et al., 2006), however, suggesting a subtle regulatory mechanism, involving multiple kinases (figure 1). Interestingly, when the Y142 tyrosine is replaced by alanine (A), creating a phospho-dead residue, binding of both CTNNA1 and BCL9L is decreased (Brembeck et al., 2004).

As CTNNB1/CTNNA1 heterodimers have been shown to be preferentially bound by CDH1 compared to monomeric CTNNB1, we hypothesize that decreasing the likelihood of CTNNB1/CTNNA1 interactions might shift the balance towards transcriptional activity, as CTNNB1 will be less likely to bind to CDH1 (Gottardi & Gumbiner, 2004). Moreover, as proposed by Gottardi & Gumbiner (2004), CTNNB1/CTNNA1 dimers could possibly be present in the nucleus (Giannini et al., 2000b, 2000a), although their communal function in the nucleus remains unknown. There are indications that it might inhibit TCF-dependent transcription (Giannini et al., 2000a), but alternatively one could speculate it to function as a buffer by segregating CTNNB1 for timely release or forming an additional route of nuclear import of CTNNB1. Taken together, targeting the CTNNB1/CTNNA1 interaction and not cell adhesion as a whole could reveal additional regulatory functions of this dimer.

Y654

Cells completely lacking CTNNA1 have been shown to still form CDH/CTNNB1 complexes (Bullions et al., 1997; Vasioukhin et al., 2001), indicating that there are multiple factors influencing CTNNB1 binding to CDH of which CTNNA1 is just one. Therefore, we also set out to mutate the Y654 residue on CTNNB1 that has been shown to be essential for CDH1 binding. Tyrosine phosphorylation of Y654 decreases the affinity of CTNNB1 for CDH. Phosphomimic mutations (glutamic acid (E)), containing a negative charge, have previously been shown to decrease CDH1 binding by at least 5-fold in both overexpression (*in vitro*) and endogenous (*in vivo*) studies (Roura et al., 1999; Tominaga et al., 2008; van Veelen et al., 2011).

By only affecting the CTNNB1/CDH binding, we hypothesize that CTNNB1/CTNNA1 binding could remain intact, depending on the order in which binding to adhesion components occurs. If CTNNB1/CTNNA1 dimers are present it is the question where these will move and what interacting partners they would bind in the absence of CDH (as CTNNB1/CTNNA1 dimers should still be able to bind TCF, albeit with lower affinity (Gottardi & Gumbiner, 2004)). Depleting CTNNB1 from the adherens junctions, but leaving the CTNNB1/CTNNA1 dimers intact could help decipher a regulatory mechanism behind the occurrence of these dimers in the nucleus.

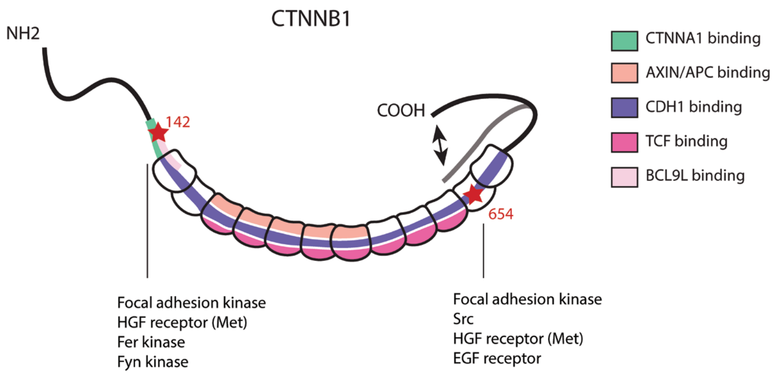

Figure 1. Regulators of the CTNNB1 binding sites

Schematic visualization of CTNNB1 and its binding sites as shown in chapter 1 (this figure was adapted to show the corresponding kinases necessary for post translational modifications). Shown are codons Y142 and Y654, which are important regulators of CTNNA1 and CDH binding, respectively. Kinases that are known to phosphorylate these residues are listed. For Y142, phosphorylation has been indicated to occur via Focal Adhesion Kinase (FAK), Hepatocyte Growth Factor (HGF) receptor (Met), and Fer and Fyn kinases, amongst others (Brembeck et al., 2004; Lilien & Balsamo, 2005; Piedra et al., 2003; Uehara & Uehara, 2021). Tyrosine phosphorylation of Y654 occurs via kinases such as Src, FAK, Hepatocyte Growth Factor (HGF) receptor (Met), and Epidermal growth factor (EGF) receptor (Lilien & Balsamo, 2005; Roura et al., 1999; Uehara & Uehara, 2021; Zeng et al., 2006).

Design and testing of gRNAs targeting the Y142 and Y654 residues

CRISPOR software was used to design multiple 20bp gRNAs to target the Y142 residue on exon 4 and the Y654 residue on exon 14 (figure 2). Guides were chosen based on specificity and efficiency according to the CRISPOR score guidelines provided by Concordet & Haeussler (2018) (table 6). MIT specificity scores (ranging 0-100), predicting the specificity of the guides and chances of off-target effects (Hsu et al., 2013), were all well above the recommended value of 50. Doench '16 efficiency scores (ranging 0-100), predicting the efficiency of cutting at the desired site using a specific guide (Doench et al., 2016), were taken into account as well, but were not leading. Where possible, guides that overlapped with the target codon were chosen (guide 241), as this prevents the gRNA from binding again after the point mutation has been occurred.

Next, we tested the individual gRNA plasmids for cutting efficiency using Tracking of Indels by Decomposition (TIDE) (supplementary figure 2 & table 6) (Brinkman et al., 2014). For the Y142 residue, the TIDE score for gRNA 238 was the highest at 19.1% (range 4.4%-19.1%) (supplementary figure 2). Disappointingly, the TIDE scores for all tested gRNAs for Y654 were quite low (1.8%-5.3%).

Table 6. CRISPOR and TIDE scores of gRNAs targeting the Y142 and Y654 residues on CTNNB1
The best gRNAs for each target codon are highlighted with an asterisk.

gRNA information			CRISPOR		TIDE
Residue	**Plasmid code**	**Target sequence**	**MIT Specificity score**	**Doench '16 efficiency score**	**TIDE score**
Y142	pRvA238	CAGTTCAGGGATTGCACGTG TGG	72	55	19.1%*
Y142	pRvA239	GACAAAACTGCTAAATGACG AGG	79	64	4.4%
Y654	pRvA240	GTGGCTTGTCCTCAGACATT CGG	74	44	1.8%
Y654	pRvA241	GCATATGTCGCTAAGAGACA AGG	81	64	5.3%*
Y654	pRvA297	AGCCGTTTCTTGTAATCTTG TGG	77	54	4.6%

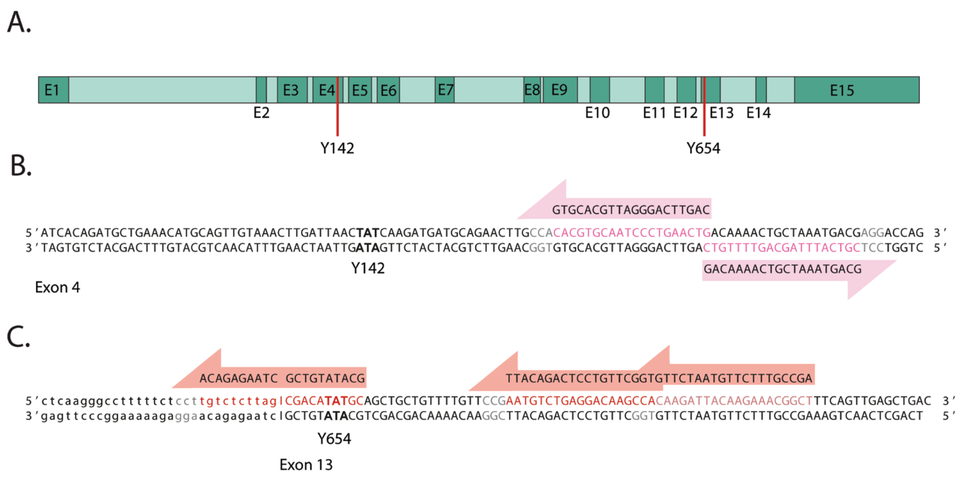

Figure 2. Designed gRNAs for Y142 and Y654 target codons
A). Schematic visualization of the CTNNB1 gene. Introns are visualized in light green, exons are numbered and visualized in dark green. The positions of the encoded target codons on CTNNB1 have been indicated. B-C). Designed gRNAs for Y142 (B) and Y654 (C), shown on top of the CTNNB1 genomic sequence. gRNAs were designed using CRISPOR and border a PAM site (NGG). Target codons are visualized in bold and respective PAM sites in dark grey. Non-coding sequence is depicted in lower case.

6

For comparison, TIDE scores were also measured for the S45F CRISPR constructs, which we had used successfully before. The TIDE score of the S45F gRNA (5.9%) is within a similar range as our best gRNA for Y654, although showing a different pattern of indels (supplementary figure 2). This illustrates that gRNAs with low scores can still lead to successful CRISPR mutations. For the most promising Y142 and Y654 guideRNAs, repair templates were designed to create Y142E and Y654E (table 3). Unfortunately, due to time constraints, these repairs have not yet been used.

We also looked into base editing as an alternative approach to CRISPR/Cas9 as this has proven a good method for creating point mutations in HAP1 cells (personal communication with Andres Lebensohn). Base editing makes use of cytosine and adenine base editors, allowing for C to T, T to C, A to G, and G to A changes (Rees & Liu, 2018). Although this does not circumvent the need of gRNAs, as the base editors are delivered via Cas9, repairs could be more efficient. Unfortunately, as we required specific point mutations (to generate Y142E, Y654E, and Y654F), base editing was not an option in this case (supplementary table 1).

Co-CRISPR trials

For chapter 4, we already created a S45F point mutation in the fluorescently tagged SGFP2-CTNNB1 HAP1 cell line (de Man et al., 2021). As the S45F mutation is known to prevent phosphorylation on residue S45 (Amit et al., 2002; Liu et al., 2002; Morin et al., 1997), it creates a constitutively active form of CTNNB1. This allowed us to screen for successful CRISPR/Cas gene editing events by FACS, as successful mutants contained high levels of SGFP2-CTNNB1 (figure 3A). For other point mutations, including Y142A/E and Y654E, the effect on CTNNB1 levels is expected to be much less prominent. As FACS screening for the mutation based on CTNNB1 signal is therefore likely to be impossible and given that endogenous tagging and mutation efficiency can be as low as 0.2% (de Man et al., 2021), this would entail manual screening by eye and/or microscopy in the hopes of observing a possible phenotype, or Sanger sequencing of many single cell clones (figure 3B). We therefore decided to optimize the co-CRISPR method, developed for use in *C. elegans* and *Drosophilla*, which makes use of the fact that two CRISPR events are likely to co-occur (Ge et al., 2016; Kane et al., 2017; Kim et al., 2014; Reuven et al., 2021). By introducing the required point mutation at the same time as the N-terminal fluorescent SGFP2 tag, successful hits can be screened based on the presence or absence of fluorescence only (figure 3C).

We aimed to find the right conditions for efficient co-CRISPR screening in human cell lines and assess the percentage of actual successful point mutations within the pool of successful fluorescently tagged cells, indicating a double hit. We first used the SGFP2-CTNNB1^{S45F} mutant in HAP1 WT cells as a model, as this would allow us to compare the success rates between different experimental conditions by screening for GFP^{low} cells in the case of a single hit (SGFP-tagging only) and GFP^{high} cells in the case of a double hit (SGFP2-tagging plus S45F point mutation).

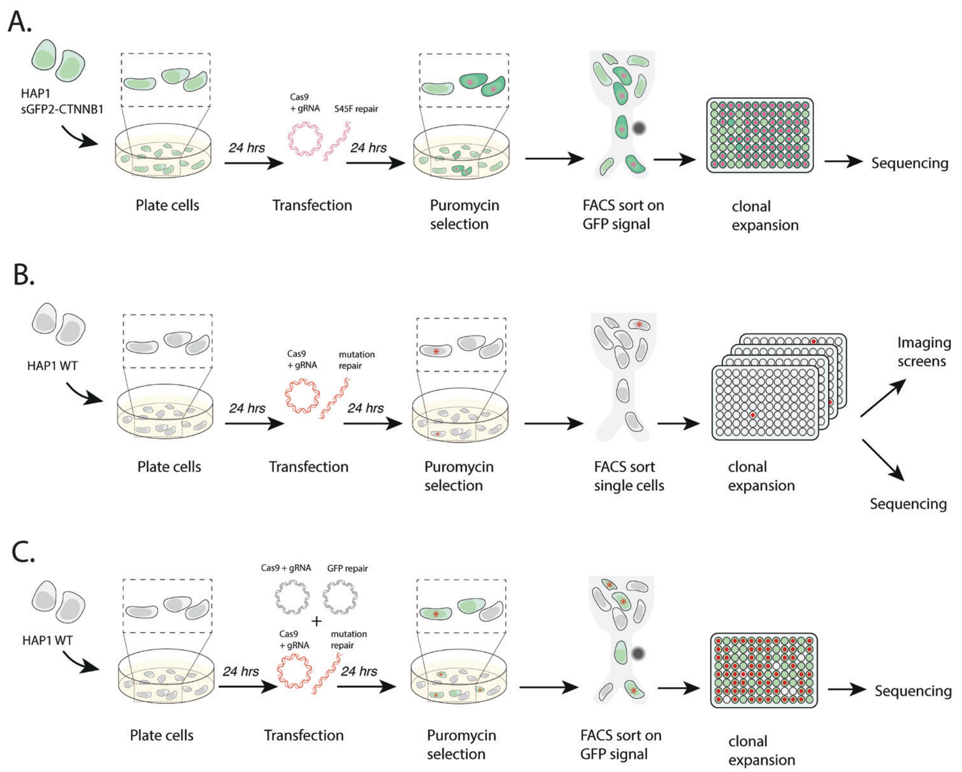

Figure 3. Schematic visualization of CRISPR and screening approaches

A). Schematic visualization of the consecutive CRISPR approach resulting in a phenotype producing point mutation. As an example, the CTNNB1 S45F point mutation is CRISPRed into a cell line in which CTNNB1 has already been fluorescently tagged. As the S45F mutation leads to hyperactivated CTNNB1, CTNNB1 levels will rise, enabling sorting on the highest GFP levels to select successful CRISPR hits. B-C). Schematic visualization of possible CRISPR approaches to create point mutations with an unknown or neutral phenotype. B). A point mutation is created and single cells are sorted. After clonal expansion, clones will have to be screened using sequencing or image-based screening, in case a morphological phenotype is present. In the case of low efficiency, a high number of clones will have to be screened to find a positive clone. C). The co-CRISPR method is applied to reduce the amount of clones to be screened for a positive hit. The creation of the point mutation is combined with fluorescent tagging and as two CRISPR events are likely to co-occur, screening for fluorescence will also likely sort out successful point mutations.

Considering that the total amount of DNA that can be transfected into a cell is ultimately limiting, we tested different ratios of the guide RNA and repair plasmids as well as different ratios of the CRISPR constructs for the SGFP2 knock-in and S45F point mutation (figure 4A). $GFP^{negative}$, GFP^{low}, and GFP^{high} populations were gated by FACS analysis based on HAP1 WT, SGFP2-CTNNB1, and SGFP2-CTNNB1^{S45F} controls, respectively (figure 4B). First, we tested different gRNA:repair ratios, whilst maintaining an equal ratio between SGFP2 and S45F constructs. The percentage of successful double hits (GFP^{high} cells) was below 0.1% in all conditions and highest for the 1:1 pX:repair ratio (0.017%) (figure 4C and table 7). We also tried different ratios between the SGFP2 and S45F constructs (keeping the gRNA:repair ratio for each at 1:1), but this did not lead to an increase in the percentage of cells with a double gene editing event. As a control, HAP1 WT cells were transfected with the SGFP2 gRNA and repair constructs only, yielding 0.4% GFP positive cells (figure 4C and table 7). For the cells that were transfected with the co-CRISPR mix, a maximum of 0.059% (lowest: 0.013%) was reached.

Table 7. Co-CRISPR trials successful single hit and double hit scores

Summary of the results of the co-CRISPR trial where different combinations of the SGFP2 and S45F CRISPR constructs were tested to optimize the protocol. The percentage of fluorescent cells, low level GFP and high level GFP cells out of the live single cell haploid population is shown. In addition, the percentage of high level GFP cells out of the fluorescent cells is shown.

Cell line	SGFP2 gRNA:repair ratio	S45F gRNA:repair ratio	SGFP2:S45F ratio	% $GFP^{positive}$ cells	% GFP^{low} cells	% GFP^{high} cells	% GFP^{high} cells out of $GFP^{positive}$ cells
HAP1 SGFP2-CTNNB1	-	1:1	-	81.4%	79.2%	1.87%	2.3%
HAP1 SGFP2-CTNNB1	-	1:2	-	92.4%	90.8%	1.17%	1.27%
HAP1 WT	1:1	-	-	0.40%	0.40%	0%	0%
HAP1 WT	1:1	1:1 (1 μl)	1:1	0.045%	0.027%	0.017%	38.9%
HAP1 WT	1:2	1:2	1:1	0.015%	0.013%	0.0025%	16.7%
HAP1 WT	2:1	2:1	1:1	0.027%	0.019%	0.0073%	27.3%
HAP1 WT	1:1	1:1	1:2	0.072%	0.059%	0.011%	15.6%
HAP1 WT	1:1	1:1	2:1	0.014%	0.014%0	0%	0%
HAP1 WT	1:1	1:1	1:3	0.048%	0.045%	0.0024%	5%
HAP1 WT	1:1	1:1 (2 μl)	1:1	0.018%	0.018%	0%	0%

To compare the efficiency of the co-CRISPR approach to a consecutive approach, the SGFP2-CTNNB1 HAP1 cell line was transfected with the S45F CRISPR constructs. The percentage of cells with a successful hit (GFP^{high} levels) out of the total amount of cells was much higher (1.17-1.87%) compared to the co-CRISPR samples (0-0.017%) (figure 4C and table 7). Although in absolute percentages the introduction of the S45F point mutation in SGFP2-CTNNB1 cells was almost 100-fold higher (max. 1.87%) than for the co-CRISPR approach (max. 0.017%), for most point mutations screening based on the strength of the GFP signal will not be possible. In that case, the double-edited cells (GFP tag plus point mutation) will be diluted in a pool of single-edited cells (GFP tag only). When this is taken into account, the percentage of GFP^{high} cells out of the total pool of edited cells (GFP^{low} + GFP^{high}) is much higher for the co-CRISPR approach (maximum 38.9%) compared to the consecutive tagging approach (2.3%) (figure 4D and table 7).

For screening purposes, co-CRISPR would thus be a more effective approach. However, it would be recommendable to start the gene editing workflow with a higher number of cells such that a sufficient number of cells with successful gene editing can be sorted. Another explanation for the drop in CRISPR efficiency when introducing multiple gene edits at the same time could be the lower amounts of DNA transfected per construct. To increase the efficiency, transfecting higher total amounts of DNA could be explored, although it is a fine line between CRISPR efficiency and cell viability due to transfection. Lastly, we do want to point out that this dataset was based on n=1 trials. Repeats of the experiment would have to point out whether the different ratios of gRNA:repair and GFP:S45F lead to the reproducible differences in efficiency.

Figure 4 (next page). Co-CRISPR optimization using SGFP2-CTNNB1 and S45F-CTNNB1 CRISPR constructs

A). Schematic representation of workflow to transfect HAP1 WT and HAP1 SGFP2-CTNNB1 with different ratios of pX:repair of each CRISPR construct and different ratios between the SGFP2 and S45F constructs. B). FACS plots showing the GFP gating in HAP1 WT, HAP1 SGFP2-CTNNB1, and HAP1 SGFP2-CTNNB1 S45F cells to set GFP positive and GFP low and high levels. Percentages of cells from the total live single haploid cell population are shown. C). FACS plots showing the GFP levels of HAP1 SGFP2-CTNNB1 cells that were transfected with S45F CRISPR constructs, HAP1 WT cells transfected with SGFP2 CRISPR constructs and HAP1 WT cells transfected with SGFP2 and S45F CRISPR constructs. Percentages of cells from the total live single haploid cell population are shown. D). Quantification of the FACS analysis of different conditions of co-CRISPR pX:repair and GFP:S45F ratios, showing the percentage of GFPhigh cells out of the total and GFPpositive population.

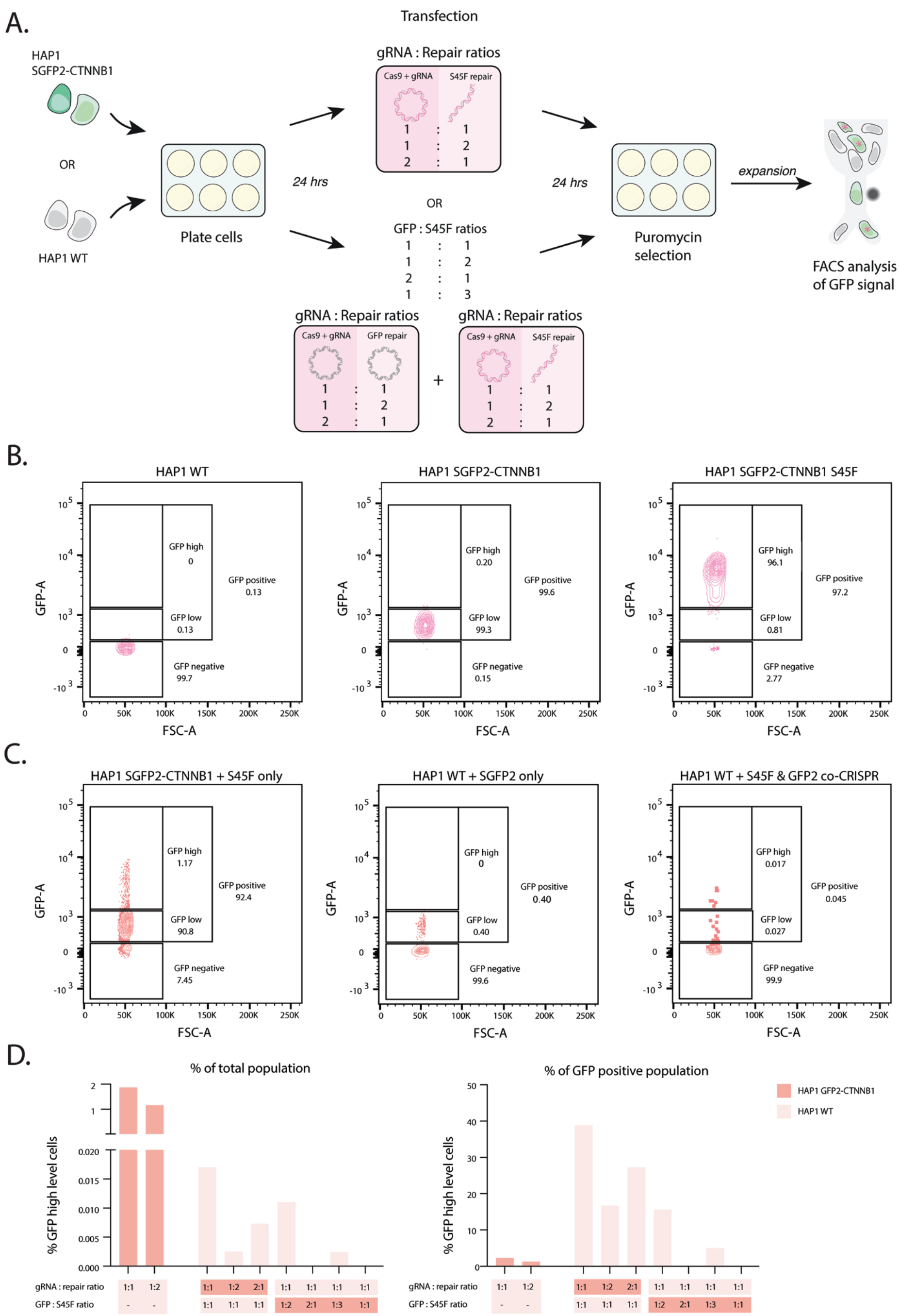
A.
Transfection
HAP1
SGFP2-CTNNB1
OR
HAP1 WT
Plate cells
24 hrs
gRNA : Repair ratios
Cas9 + gRNA
S45F repair
1 : 1
1 : 2
2 : 1
OR
GFP : S45F ratios
1 : 1
1 : 2
2 : 1
1 : 3
gRNA : Repair ratios
Cas9 + gRNA
GFP repair
+
24 hrs
Puromycin selection
expansion
FACS analysis of GFP signal
B.
HAP1 WT
HAP1 SGFP2-CTNNB1
HAP1 SGFP2-CTNNB1 S45F
GFP high
GFP low
GFP positive
GFP negative
GFP-A
FSC-A
C.
HAP1 SGFP2-CTNNB1 + S45F only
HAP1 WT + SGFP2 only
HAP1 WT + S45F & GFP2 co-CRISPR
D.
% of total population
% of GFP positive population
% GFP high level cells
HAP1 GFP2-CTNNB1
HAP1 WT
gRNA : repair ratio
GFP : S45F ratio

MCF10A CRISPR optimization: the end of the journey

The HAP1 cell line lends itself well for endogenous screening, mutating and tagging due to its near haploidy and ability to grow as single cells (as excellently reviewed by Llargués-Sistac et al. (2023)). Since the myeloid leukemic origin of HAP1 cells is hematopoietic (Andersson et al., 1987; Carette et al., 2011; Kotecki et al., 1999), we aspired to move to a more physiologically relevant epithelial cell line with CDH1-containing junctions such as the non-transformed near-diploid human breast epithelial MCF10A cells (Soule et al., 1990). In this system we hoped to combine the Y142 and Y654 point mutations with fluorescent tagging of CTNNB1 with SGFP2 and mEos4B, a photoconvertible green-to-red fluorescent protein (for a more elaborate description of which the reader is referred to the general discussion of this thesis). Unfortunately, we encountered multiple hurdles in our attempts to tag and mutate CTNNB1 in MCF10A, including low transfection efficiency of our MCF10A cells and difficulty to grow from single cells, a prerequisite for clonal selection after gene editing.

As for making the Y142 and Y654 point mutations, we needed monoclonal CRISPR lines, we experimented with various methods to stimulate single cell growth post FACS sorting, as listed in table 8. Most of these approaches together with the inefficient transfection of CRISPR constructs proved insufficient to allow for further tagging and screening. In one attempt to obtain a monoclonal mEos4B-CTNNB1 MCF10A line (a green fluorescent photoconvertible protein), cells were transfected with mEos4B-CTNNB1 CRISPR constructs and single GFP^{positive} cells were sorted into a well with a WT MCF10A population to allow paracrine signalling. By allowing the full population to grow out and resorting the resulting population (WT and GFP^{positive} MCF10A), we were able to recover a sufficiently large number of GFP^{positive} cells that originated from a single clone. However, subsequent PCRs and sequencing of this population surprisingly did not confirm a successful CRISPR event. This practical roadblock ultimately prevented us from performing co-CRISPR in MCF10A cells.

6

Table 8. MCF10A single cell sorting optimization solutions

Solutions to increase the single cell viability of MCF10A cells post FACS sorting and the corresponding result on single cell viability.

Solution	Result
Coating plates O/N with 0.1% gelatin	No increase in single cell viability
Coating plates O/N with fibronectin	No increase in single cell viability
Sorting GFP+ cells into a WT population of MCF10A cells to grow out and resort later	Increased viability of sorted cells and a successful resort of a larger GFP+ population coming from a single cell
Spinning down plate after sorting (4 min at 1000 rpm)	No increase in single cell viability
ROCK inhibitor	No increase in single cell viability
Increasing FBS percentage in HF solution during FACS	No increase in single cell viability
Sorting into conditioned medium	No increase in single cell viability

Summary & outlook

In this chapter, we laid the foundation for endogenous creation of the Y142E and Y654E point mutations in CTNNB1, using co-CRISPR for effective screening. As we experienced, unfortunately, not every cell type lends itself for efficient transfection and single cell screening, which is why this project was cut short due to time constraints. However, we still believe these mutations could help dissect the regulation of the balance of CTNNB1 and interaction between the two functions via CTNNB1 and hope this chapter can be used as a starting point for future endeavours. For the MCF10A cells, low level (lentiviral) overexpression of tagged CTNNB1 constructs containing the desired point mutations could be an alternative to the CRISPR/Cas9 approach. As shown by Kafri et al. (2016), overexpressing CTNNB1 at sub-endogenous levels (leading to a 2-fold increase of total CTNNB1 levels) retains normal CTNNB1 dynamics in response to WNT stimulation and CTNNB1 functionality in adherens junctions. As to not dilute the effects of the point mutations in the endogenous CTNNB1 background, using low level overexpression for mutated CTNNB1 would require a knock-down of the endogenous background. To achieve this, we would recommend using shRNAs to create a CTNNB1 knockdown, as a knockout could potentially create a partial, hyperactive form of CTNNB1. Ideally, the knockdown would be inducible by for example doxycycline, to observe changes in CTNNB1 localization upon full dependence on mutated CTNNB1. Additionally, this approach might improve cell viability when culturing the cells that contain the mutated CTNNB1 as it remains a possible scenario that the point mutations suggested here lead to completely dysfunctional adherens junctions. In this case, an inducible system could still show a balance shift, but would allow a healthy starting point for each experiment. All in all, this chapter has shown that balancing optimal experimental design and practical feasibility remains as much of a balancing act as balancing CTNNB1 between its functional pools.

Acknowledgements

We thank Gonzalo Congrains Sotomayor for his help with the FACS experiments.

Author contributions

TvdW – conceptualization, experimental design, experimental execution (FACS sample preparation) and supervision of MR, data curation, visualization and analysis (gRNA design, FACS data), manuscript writing

MR – Experimental execution (cell culture, FACS sample preparation, cloning, CRISPR),

analysis (TIDE analysis), manuscript inspiration (these results were first written down by MR as a student report. Parts of this report were taken as inspiration for this chapter)
SdM – conceptualization (S45F CRISPR approach), experimental design (designed the first Y142 and Y654 gRNAs and designed the S45F gRNA)
RvA – conceptualization, supervision, manuscript review and editing

References

Aberle, H., Butz, S., Stappert, J., Weissig, H., Kemler, R., & Hoschuetzky, H. (1994). Assembly of the cadherin-catenin complex in vitro with recombinant proteins. *Journal of Cell Science*, *107*(12), 3655–3663. https://doi.org/10.1242/jcs.107.12.3655

Aberle, H., Schwartz, H., Hoschuetzky, H., & Kemler, R. (1996). Single Amino Acid Substitutions in Proteins of the *armadillo* Gene Family Abolish Their Binding to α-Catenin. *Journal of Biological Chemistry*, *271*(3), 1520–1526. https://doi.org/10.1074/jbc.271.3.1520

Amit, S., Hatzubai, A., Birman, Y., Andersen, J. S., Ben-Shushan, E., Mann, M., Ben-Neriah, Y., & Alkalay, I. (2002). Axin-mediated CKI phosphorylation of β-catenin at Ser 45: A molecular switch for the Wnt pathway. *Genes & Development*, *16*(9), 1066–1076. https://doi.org/10.1101/gad.230302

Andersson, B. S., Beran, M., Pathak, S., Goodacre, A., Barlogie, B., & McCredie, K. B. (1987). Ph-positive chronic myeloid leukemia with near-haploid conversion in vivo and establishment of a continuously growing cell line with similar cytogenetic pattern. *Cancer Genetics and Cytogenetics*, *24*(2), 335–343. https://doi.org/10.1016/0165-4608(87)90116-6

Brembeck, F. H., Schwarz-Romond, T., Bakkers, J., Wilhelm, S., Hammerschmidt, M., & Birchmeier, W. (2004). Essential role of BCL9-2 in the switch between β-catenin's adhesive and transcriptional functions. *Genes & Development*, *18*(18), 2225–2230. https://doi.org/10.1101/gad.317604

Brinkman, E. K., Chen, T., Amendola, M., & van Steensel, B. (2014). Easy quantitative assessment of genome editing by sequence trace decomposition. *Nucleic Acids Research*, *42*(22), e168. https://doi.org/10.1093/nar/gku936

Bullions, L. C., Notterman, D. A., Chung, L. S., & Levine, A. J. (1997). Expression of wild-type alpha-catenin protein in cells with a mutant alpha-catenin gene restores both growth regulation and tumor suppressor activities. *Molecular and Cellular Biology*, *17*(8), 4501–4508. https://doi.org/10.1128/MCB.17.8.4501

Carette, J. E., Raaben, M., Wong, A. C., Herbert, A. S., Obernosterer, G., Mulherkar, N., Kuehne, A. I., Kranzusch, P. J., Griffin, A. M., Ruthel, G., Cin, P. D., Dye, J. M., Whelan, S. P., Chandran, K., & Brummelkamp, T. R. (2011). Ebola virus entry requires the cholesterol transporter Niemann–Pick C1. *Nature*, *477*(7364), 340–343. https://doi.org/10.1038/nature10348

Concordet, J.-P., & Haeussler, M. (2018). CRISPOR: Intuitive guide selection for CRISPR/Cas9 genome editing experiments and screens. *Nucleic Acids Research*, *46*(W1), W242–W245. https://doi.org/10.1093/nar/gky354

de Man, S. M., Zwanenburg, G., van der Wal, T., Hink, M. A., & van Amerongen, R. (2021). Quantitative live-cell imaging and computational modeling shed new light on endogenous WNT/CTNNB1 signaling dynamics. *eLife*, *10*, e66440. https://doi.org/10.7554/eLife.66440

Doench, J. G., Fusi, N., Sullender, M., Hegde, M., Vaimberg, E. W., Donovan, K. F., Smith, I., Tothova, Z., Wilen, C., Orchard, R., Virgin, H. W., Listgarten, J., & Root, D. E. (2016). Optimized sgRNA design to maximize activity and minimize off-target effects of CRISPR-Cas9. *Nature Biotechnology*, *34*(2), 184–191. https://doi.org/10.1038/nbt.3437

Ge, D. T., Tipping, C., Brodsky, M. H., & Zamore, P. D. (2016). Rapid Screening for CRISPR-Directed Editing of the Drosophila Genome Using white Coconversion. *G3: Genes|Genomes|Genetics*, *6*(10), 3197–3206. https://doi.org/10.1534/g3.116.032557

Giannini, A. L., Vivanco, M. d, & Kypta, R. M. (2000a). Alpha-catenin inhibits beta-catenin signaling by preventing formation of a beta-catenin*T-cell factor*DNA complex. *The Journal of Biological Chemistry*, *275*(29), 21883–21888. https://doi.org/10.1074/jbc.M001929200

Giannini, A. L., Vivanco, M. M., & Kypta, R. M. (2000b). Analysis of beta-catenin aggregation and localization using GFP fusion proteins: Nuclear import of alpha-catenin by the beta-catenin/Tcf complex. *Experimental Cell Research*, *255*(2), 207–220. https://doi.org/10.1006/excr.1999.4785

Gottardi, C. J., & Gumbiner, B. M. (2004). Distinct molecular forms of β-catenin are targeted to adhesive or transcriptional complexes. *Journal of Cell Biology*, *167*(2), 339–349. https://doi.org/10.1083/jcb.200402153

Hoffmans, R., & Basler, K. (2007). BCL9-2 binds Arm/β-catenin in a Tyr142-independent manner and requires Pygopus for its function in Wg/Wnt signaling. *Mechanisms of Development*, *124*(1), 59–67. https://doi.org/10.1016/j.mod.2006.09.006

Hsu, P. D., Scott, D. A., Weinstein, J. A., Ran, F. A., Konermann, S., Agarwala, V., Li, Y., Fine, E. J., Wu, X., Shalem, O., Cradick, T. J., Marraffini, L. A., Bao, G., & Zhang, F. (2013). DNA targeting specificity of RNA-guided Cas9 nucleases. *Nature Biotechnology*, *31*(9), 827–832. https://doi.org/10.1038/nbt.2647

Kafri, P., Hasenson, S. E., Kanter, I., Sheinberger, J., Kinor, N., Yunger, S., & Shav-Tal, Y. (2016). Quantifying β-catenin subcellular dynamics and cyclin D1 mRNA transcription during Wnt signaling in single living cells. *eLife*, *5*, e16748. https://doi.org/10.7554/eLife.16748

Kane, N. S., Vora, M., Varre, K. J., & Padgett, R. W. (2017). Efficient Screening of CRISPR/Cas9-Induced Events in Drosophila Using a Co-CRISPR Strategy. *G3 Genes|Genomes|Genetics*, *7*(1), 87–93. https://doi.org/10.1534/g3.116.036723

Kim, H., Ishidate, T., Ghanta, K. S., Seth, M., Conte, D., Jr., Shirayama, M., & Mello, C. C. (2014). A Co-CRISPR Strategy for Efficient Genome Editing in Caenorhabditis elegans. *Genetics*, *197*(4), 1069–1080. https://doi.org/10.1534/genetics.114.166389

Kotecki, M., Reddy, P. S., & Cochran, B. H. (1999). Isolation and Characterization of a Near-Haploid Human Cell Line. *Experimental Cell Research*, *252*(2), 273–280. https://doi.org/10.1006/excr.1999.4656

Lilien, J., & Balsamo, J. (2005). The regulation of cadherin-mediated adhesion by tyrosine phosphorylation/dephosphorylation of β-catenin. *Current Opinion in Cell Biology*, *17*(5), 459–465. https://doi.org/10.1016/j.ceb.2005.08.009

Liu, C., Li, Y., Semenov, M., Han, C., Baeg, G.-H., Tan, Y., Zhang, Z., Lin, X., & He, X. (2002). Control of β-Catenin Phosphorylation/Degradation by a Dual-Kinase Mechanism. *Cell*, *108*(6), 837–847. https://doi.org/10.1016/S0092-8674(02)00685-2

Llargués-Sistac, G., Bonjoch, L., & Castellvi-Bel, S. (2023). HAP1, a new revolutionary cell model for gene editing using CRISPR-Cas9. *Frontiers in Cell and Developmental Biology*, *11*, 1111488. https://doi.org/10.3389/fcell.2023.1111488

Morin, P. J., Sparks, A. B., Korinek, V., Barker, N., Clevers, H., Vogelstein, B., & Kinzler, K. W. (1997). Activation of β-Catenin-Tcf Signaling in Colon Cancer by Mutations in β-Catenin or APC. *Science*, *275*(5307), 1787–1790. https://doi.org/10.1126/science.275.5307.1787

Piedra, J., Miravet, S., Castaño, J., Pálmer, H. G., Heisterkamp, N., García de Herreros, A., & Duñach, M. (2003). P120 Catenin-Associated Fer and Fyn Tyrosine Kinases Regulate β-Catenin Tyr-142 Phosphorylation and β-Catenin-α-Catenin Interaction. *Molecular and Cellular Biology*, *23*(7), 2287–2297. https://doi.org/10.1128/MCB.23.7.2287-2297.2003

Ran, F. A., Hsu, P. D., Wright, J., Agarwala, V., Scott, D. A., & Zhang, F. (2013). Genome engineering using the CRISPR-Cas9 system. *Nature Protocols*, *8*(11), 2281–2308. https://doi.org/10.1038/nprot.2013.143

Rees, H. A., & Liu, D. R. (2018). Base editing: Precision chemistry on the genome and transcriptome of living cells. *Nature Reviews. Genetics*, *19*(12), 770–788. https://doi.org/10.1038/s41576-018-0059-1

Reuven, N., Adler, J., Myers, N., & Shaul, Y. (2021). CRISPR Co-Editing Strategy for Scarless Homology-Directed Genome Editing. *International Journal of Molecular Sciences*, *22*(7), Article 7. https://doi.org/10.3390/ijms22073741

Roura, S., Miravet, S., Piedra, J., García de Herreros, A., & Duñach, M. (1999). Regulation of E-cadherin/Catenin association by tyrosine phosphorylation. *The Journal of Biological Chemistry*, *274*(51), 36734–36740. https://doi.org/10.1074/jbc.274.51.36734

Sampietro, J., Dahlberg, C. L., Cho, U. S., Hinds, T. R., Kimelman, D., & Xu, W. (2006). Crystal structure of a beta-catenin/BCL9/Tcf4 complex. *Molecular Cell*, *24*(2), 293–300. https://doi.org/10.1016/j.molcel.2006.09.001

Soule, H. D., Maloney, T. M., Wolman, S. R., Peterson, W. D., Brenz, R., McGrath, C. M., Russo, J., Pauley, R. J., Jones, R. F., & Brooks, S. C. (1990). Isolation and characterization of a spontaneously immortalized human breast epithelial cell line, MCF-10. *Cancer Research*, *50*(18), 6075–6086.

Tominaga, J., Fukunaga, Y., Abelardo, E., & Nagafuchi, A. (2008). Defining the function of β-catenin tyrosine phosphorylation in cadherin-mediated cell–cell adhesion. *Genes to Cells*, *13*(1), 67–77. https://doi.org/10.1111/j.1365-2443.2007.01149.x

Uehara, K., & Uehara, A. (2021). Immunohistochemical study of dissociation and association of adherens junctions in splenic sinus endothelial cells. *Cell and Tissue Research*, *384*(1), 25–33. https://doi.org/10.1007/s00441-021-03426-7

van Veelen, W., Le, N. H., Helvensteijn, W., Blonden, L., Theeuwes, M., Bakker, E. R. M., Franken, P. F., van Gurp, L., Meijlink, F., van der Valk, M. A., Kuipers, E. J., Fodde, R., & Smits, R. (2011). β-catenin tyrosine 654 phosphorylation increases Wnt signalling and intestinal tumorigenesis. *Gut*, *60*(9), 1204–1212. https://doi.org/10.1136/gut.2010.233460

Vasioukhin, V., Bauer, C., Degenstein, L., Wise, B., & Fuchs, E. (2001). Hyperproliferation and defects in epithelial polarity upon conditional ablation of alpha-catenin in skin. *Cell*, *104*(4), 605–617. https://doi.org/10.1016/s0092-8674(01)00246-x

Zeng, G., Apte, U., Micsenyi, A., Bell, A., & Monga, S. P. S. (2006). Tyrosine residues 654 and 670 in beta-catenin are crucial in regulation of Met-β-catenin interactions. *Experimental Cell Research*, *312*(18), 3620–3630. https://doi.org/10.1016/j.yexcr.2006.08.003

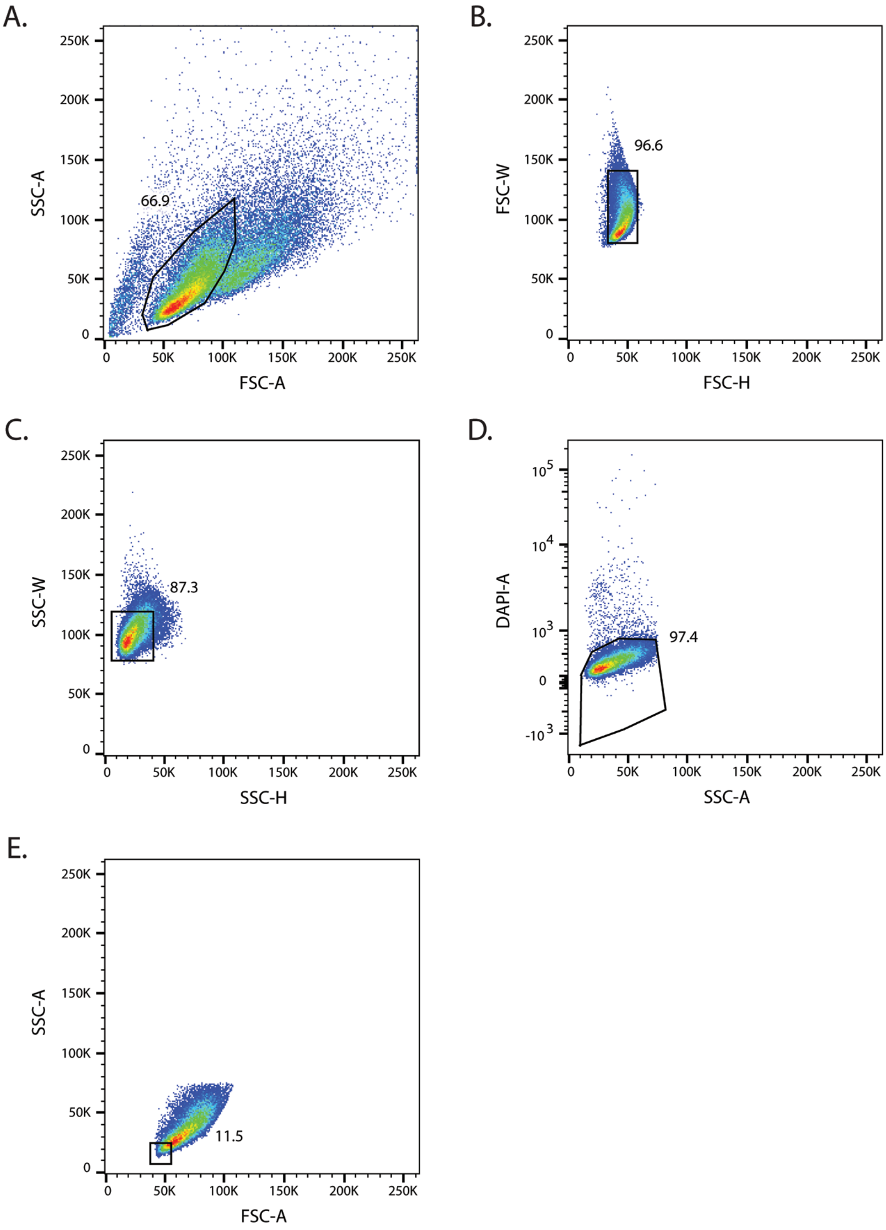

Supplementary figure 1. Gating strategy for FACS analysis to create a population of single live haploid cells

Single, live cells were gated based on WT and DAPI stained dead WT cells. Subsequently, haploid cells were backgated based on size. From this population, GFP positive cells were counted and divided into low level and high levels categories based on control samples. A-C). SSC-A versus FSC-A, FSC-W versus FSC-H and SSC-W versus SSC-H gating steps based on size and granularity to get a single cell population. D). Gating on DAPI signal to get a population of live cells. E). SSC-A versus FSC-A back gating based on size and granularity to get the haploid population.

Supplementary table 1. Options for base-editing mutation on the Y142 and Y654 residues

The desired mutations at target codons Y142 and Y654 are listed. For every mutation, several sequence options exist, which are listed. For every option, the bases that differ from the original sequence are underlined. These changes are listed below, with the ones that are possible through base editing in green and changes that are not possible through base editing in red.

Target codon	Mutation	Original sequence	Mutated sequence options				Base editing
Y142	Y142E	TAT	GAA	GAG			NO
			T > G	T > G			
			T > A	T > G			
Y142	Y142A	TAT	GCT	GCC	GCA	GCG	NO
			T > G	T > G	T > G	T > G	
			A > C	A > C	A > C	A > C	
				T > C	T > A	T > G	
Y142	Y142F	TAT	TTT	TTC	TTA	TTG	NO
			A > T	A > T	A > T	A > T	
				T > C	T > A	T > G	
Y654	Y654E	TAT	GAA	GAG			NO
			T > G	T > G			
			T > A	T > G			
Y654	Y654F	TAT	TTT	TTC	TTA	TTG	NO
			A > T	A > T	A > T	A > T	
				T > C	T > A	G > T	

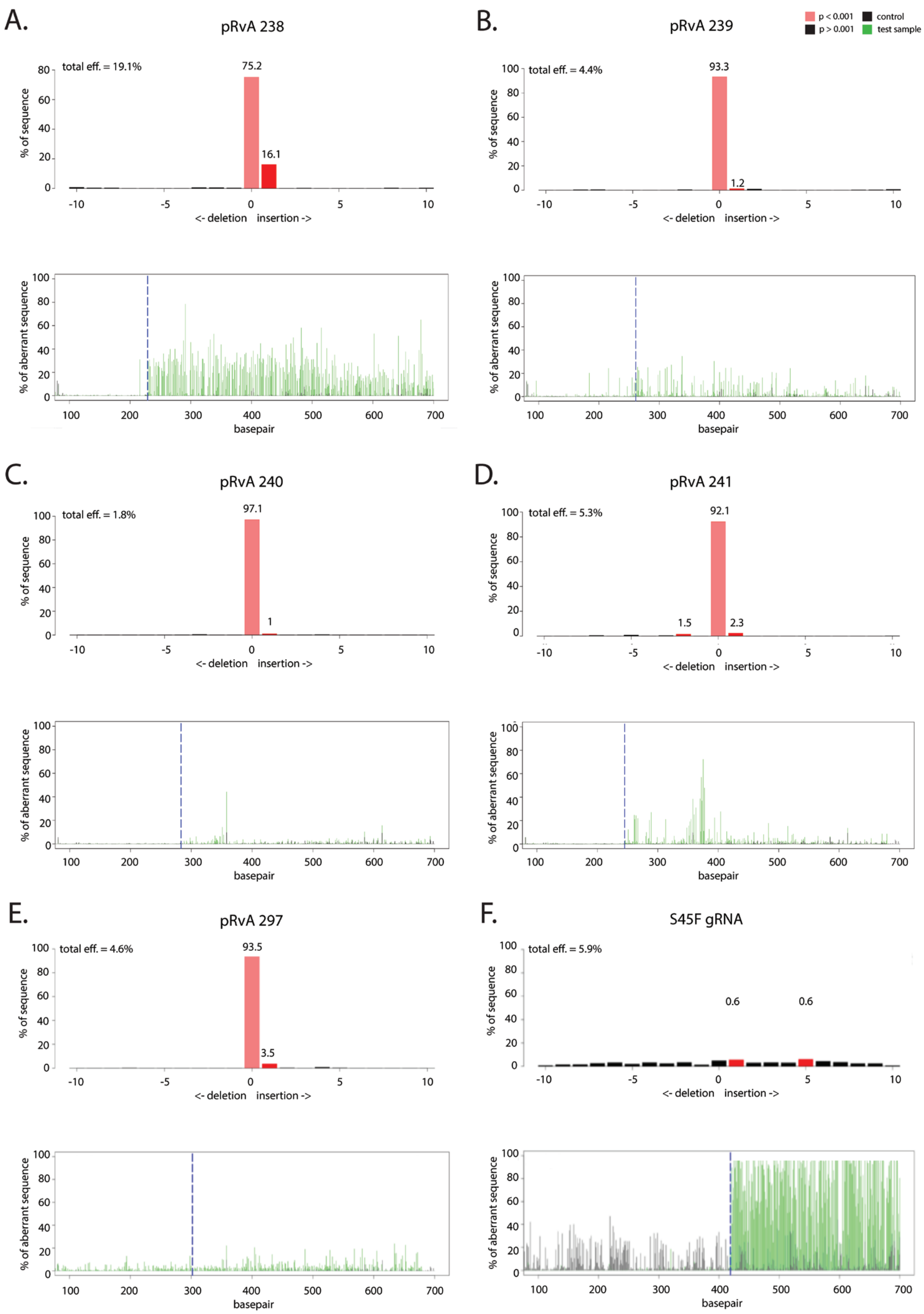
A.
pRvA 238
total eff. = 19.1%
75.2
16.1
% of sequence
<- deletion insertion ->
% of aberrant sequence
basepair
B.
pRvA 239
p < 0.001
p > 0.001
control
test sample
total eff. = 4.4%
93.3
1.2
C.
pRvA 240
total eff. = 1.8%
97.1
1
D.
pRvA 241
total eff. = 5.3%
92.1
1.5
2.3
E.
pRvA 297
total eff. = 4.6%
93.5
3.5
F.
S45F gRNA
total eff. = 5.9%
0.6
0.6

Supplementary figure 2 (left). TIDE results for Y142 and Y654 target codons gRNAs

TIDE (Tracking of Indels by Decomposition) analysis results (Brinkman et al., 2014) for gRNAs targeting Y142 (A-B) and Y654 (C-E). As a reference the TIDE result for the gRNA used to target S45F (F) is shown. Bar graphs in the top panel show the indel spectrum (red bars $p < 0.001$ and black bars $p > 0.001$). The bottom panel shows the aberrant sequence signal (test sample in green and control sample in black) quality control, with the expected cut site located at the dashed blue line.